

## Performance evaluation of alumina trihydrate and silica-filled silicone rubber composites for outdoor high-voltage insulations

Hidayatullah KHAN<sup>1,\*</sup>, Muhammad AMIN<sup>2</sup>, Ayaz AHMAD<sup>1</sup>

<sup>1</sup>Department of Electrical Engineering, COMSATS Institute of Information Technology, Wah Cantt, Punjab, Pakistan

<sup>2</sup>Department of Electrical Engineering, Ghulam Ishaq Khan Institute of Engineering Sciences and Technology, Topi, Khyber Pakhtunkhwa, Pakistan

Received: 28.09.2016

Accepted/Published Online: 08.06.2018

Final Version: 28.09.2018

**Abstract:** In recent years, silicone rubber-based composites have been widely investigated for outdoor applications due to their promising insulating properties. However, mechanical, thermal, and tracking properties of pure silicone rubber are very poor, which restrains its application for long-term performance. In this research work, the influence of microsized alumina trihydrate (ATH) and micro/nanosized silica (SiO<sub>2</sub>) fillers on mechanical, thermal, and electrical properties of room temperature vulcanized silicone rubber (RTV-SiR) has been studied. SiR-blends with varying amounts of ATH and SiO<sub>2</sub> particles were prepared by blending in a two-roll mixing mill, compression molding, and postcuring processes in sequence. In order to evaluate relative tracking and erosion resistance of SiR-blends, an inclined plane test (IPT) was conducted in accordance with the ASTM D2303 standard procedure. Surface temperature distribution was recorded using a Fluke-Ti25 infrared camera during IPT experiments. Thermogravimetric analysis was carried out to analyze the thermal stability of ATH and silica-filled silicone rubber samples. Tensile strength, percent elongation at break, hardness, erosion, tracking resistance, and thermal properties were also investigated and discussed. Results showed that the mechanical, thermal, tracking, and erosion performances of SiR-blends are improved by the incorporation of ATH and silica particles, which is governed by filler type, size, and wt.% in the polymer matrix.

**Key words:** Alumina trihydrate, inclined plane test, characterization, silicone rubber, silica

### 1. Introduction

Since the 1970s, silicone rubber (SiR) has been used for outdoor insulation [1]. Due to its light weight, unique hydrophobicity, better pollution/contamination performance, easy installation, and excellent insulation properties (resistivity of  $>10^{12}\Omega$ ), SiR composite insulators are broadly employed in high-voltage (HV) transmission and distribution [2]. However, these polymeric materials are affected by various types of environmental and electrical stresses, which limit their use as HV insulants [3,4]. Heavy rain, ultraviolet radiation (UV), pollution, dry band arcing, corona discharge, temperature, chemicals, cyclic loads, and moisture penetration play significant roles in SiR degradation [5]. In addition, the tracking and erosion of polymer insulants due to dry band arcing is the other main problem that has not yet been fully addressed [6]. During service, if the localized surface temperature due to dry band arcing becomes greater than the insulant's safe limit, a chemical reaction may take place, which can lead to material tracking and erosion [7].

\*Correspondence: [hidayat.msk@gmail.com](mailto:hidayat.msk@gmail.com)

In order to enhance the mechanical, thermal, and tracking properties of pure SiR insulants, making these promising candidates for HV outdoor applications, inorganic particle incorporation in the base material has received the focused attention of researchers. Improvement in the physical and electrical properties due to incorporation of micro- and nanosized particles motivated researchers to try different types as well as sizes of fillers so as to optimize their performance as insulants [8–11]. Furthermore, inorganic particles build a barrier to avoid surface tracking and hinder insulator surface erosion as a result of heat produced during dry band arcing, thus preventing material degradation [12]. Previously,  $\text{Fe}_2\text{O}_3$  [13],  $\text{Al}_2\text{O}_3$  [14], carbon black, titanium dioxide, magnesium oxide, calcium carbonate, ZnO, etc. were dispersed in SiR matrixes and investigated [15–17]. However, these fillers are costly and susceptible to acid attack. Alumina trihydrate (ATH) and natural silica have also been frequently incorporated into SiR matrixes to tweak mechanical, thermal, tracking, and erosion resistance properties [7,18,19]. This reinforcement is the function of filler size, shape, and dispersion as well as molecular interactions [20].

Recently, synthesis, design, thermal degradation, and erosion resistance of SiR composites were reported in a number of studies [11,21–29]. Du et al. [21] reported that material degradation depends on leakage current magnitude and arc mobility. Likewise, Ansoorge et al. [22] found that at high temperature (350 °C for pure SiR), thermal degradation of SiR composites is due to depolymerization and formation of low-molecular-weight components, which varies with pollution density and polymer functional groups. According to Meyer et al. [23] the particle size, shape, and particle/polymer bond potential are the most significant features of inorganic fillers to improve the polymer characteristics (electrical, mechanical, and thermal). Furthermore, the authors of [24] investigated the impact of particle size, its surface modification, and tracking resistances. In another work Du et al. [25] studied the influence of thermal conductivity on DC resistance to erosion of SiR/BN nanocomposites. They inferred that with the increase in particle concentration from 0 to 7 wt.% thermal conductivity was enhanced, thereby reducing the weight loss and erosion. Likewise, the authors of [26] examined the effect of barium titanate ( $\text{BaTiO}_3$ ) on surface degradation and tracking resistance of room temperature vulcanized (RTV)-SiR composites. Isaias et al. [11] investigated inclined plane tests (IPTs) on ATH and silica-filled composites with SiR and EPDM to evaluate the effect of inorganic particles on erosion/tracking resistance of SiR and EPDM composites. According to Refat et al. [27], the dry band arcing and erosion of SiR can be suppressed by incorporating ATH and silica particles in the DC-IPT using wavelet-based multiresolution analysis of leakage current. Likewise, it was found that particles in networked dispersion in a polymer matrix can improve the composite properties [28].

This work is the continuation of our previous work in which we investigated the impact of silica particles on mechanical, thermal, and electrical properties of EPDM, epoxy, and SiR composites [29]. However, AC-IPT-based analysis of ATH and silica particle-filled SiR composites has not been thoroughly investigated before to the best of our knowledge. The investigated SiR composite insulants showed high tracking and erosion resistance as well as enhanced mechanical and thermal properties, indicating great potential for electronic and electrical engineering applications, such as HV transmission and substation insulation. Samples of SiR mixed with microsized ATH, microsized  $\text{SiO}_2$ , microsized (ATH +  $\text{SiO}_2$ ), and (microsized ATH + nanosized  $\text{SiO}_2$ ) particles with different wt.% ATH/ $\text{SiO}_2$  were prepared and investigated using IPT analysis in this study. The performance metrics studied include tensile strength, % elongation at break (%EAB), hardness, weight loss with temperature, and erosion/tracking resistance properties of SiR novel blends. The synergetic impact of micro-ATH and micro/nanosized- $\text{SiO}_2$  fillers and their wt.% on the overall performance of SiR-blends are discussed.

## 2. Experimental

### 2.1. Materials

In this work the base material, RTV-SiR (70% polydimethylsiloxane and 30% vinyl), with density of  $1.15 \text{ g cm}^{-3}$  was supplied by Wacker Chemie (Germany). The micro-ATH, micro-SiO<sub>2</sub>, and nano-SiO<sub>2</sub> fillers were produced by Huber Engineering Materials, US-Silica, and Sigma-Aldrich, respectively. In addition, different physical properties of ATH and silica particles are tabulated in Table 1. Moreover, various auxiliary chemicals like sulfur, ZnO, and stearic-acid were commercially available and purchased from the local market. The chemical structures of ATH, SiO<sub>2</sub>, and SiR are shown in Figures 1a–1c, respectively.

**Table 1.** Particle specifications.

Particle	Average particle size	Surface area/g (m <sup>2</sup> /g, BET)	pH	Purity (%)	Supplier
Micro-ATH	5 $\mu\text{m}$	3.5	9	99	Huber Engineering Materials
Micro-SiO <sub>2</sub>	3 $\mu\text{m}$	5	6.2	99.5	US Silica
Nano-SiO <sub>2</sub>	10 nm	390	6.5	99.8	Sigma-Aldrich

### 2.2. Blends preparation

Preparation of RTV-SiR composites was performed in a high shear blender (HSM-100LSK) via simple blending followed by hot compression molding and postcuring technique. Blending of SiR and inorganic-particles (ATH/SiO<sub>2</sub>) with known quantities of activator and accelerators was carried out in a two-roll mixing mill using the ASTM D1418-10a standard procedure [30]. During mixing the mixer speed, mixing duration, and temperature were kept as 50 rpm, 20 min, and 150 °C, respectively. Thereafter, the amalgamated mixture was poured into a preheated steel mold (circular shape, 3.5 mm thick, and 85 mm in diameter), following by compression molding in a hydraulic press at 20 MPa for 30 min. ZnO, tetramethylthiuram-disulfide, stearic acid and mercapto-benzothiazole were used as auxiliary additives. Chemical compositions of doped and undoped SiR samples are summarized in Table 2.

### 2.3. Blends characterization

#### 2.3.1. Mechanical characterization

Mechanical properties such as tensile strength (TS) and %EAB were measured using a universal testing machine (Instron-4465) with a 25 mm/min cross-head speed at room temperature according to ASTM D412 [31]. Samples used were shaped as per standard requirements. TS and %EAB can be calculated using the following equations [32]:

$$TS(MPa) = P/A, \quad (1)$$

$$EAB(\%strain) = E/L \times 100, \quad (2)$$

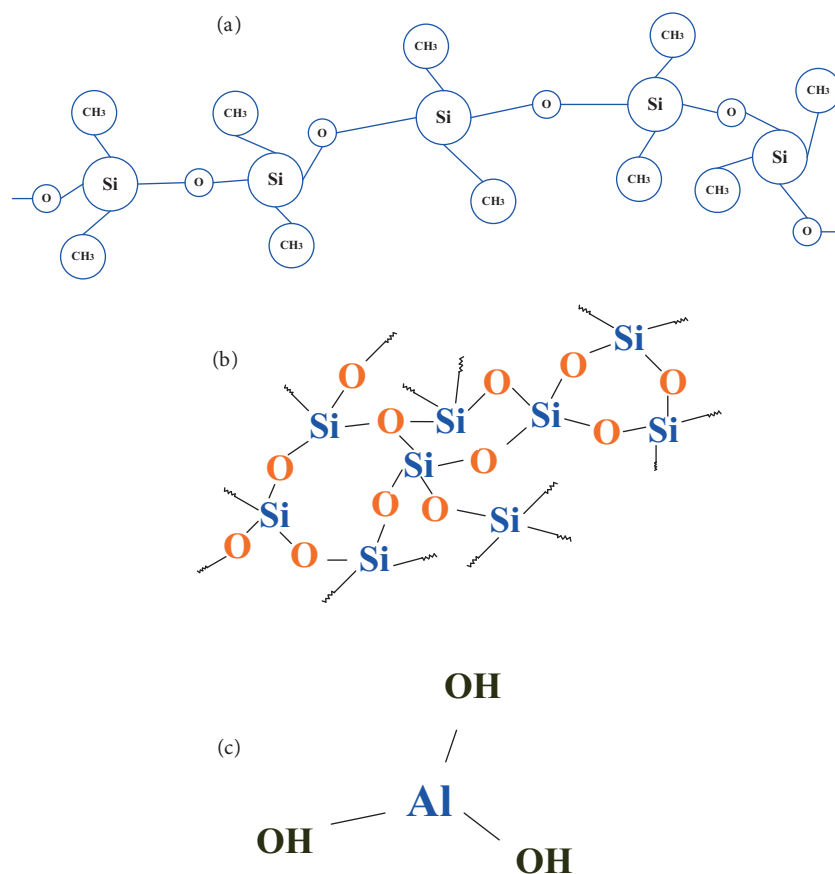


**Figure 1.** Chemical structure of (a) SiR, (b) SiO<sub>2</sub>, and (c) ATH.

**Table 2.** Prepared samples' chemical composition.

Blend code	Description	Base material	Inorganic particles		
			Type	size	Concentration [wt.%]
A	Neat SiR	RTV-SiR	-	-	-
B	15% $\mu$ ATH+SiR	RTV-SiR	ATH	5 $\mu$ m	15
C	20% $\mu$ ATH+SiR	RTV-SiR	ATH	5 $\mu$ m	20
D	15% $\mu$ ATH+5% $\mu$ SiO <sub>2</sub> +SiR	RTV-SiR	ATH	5 $\mu$ m	15
			SiO <sub>2</sub>	3 $\mu$ m	5
E	10% $\mu$ ATH+2% nSiO <sub>2</sub> +SiR	RTV-SiR	ATH	5 $\mu$ m	10
			SiO <sub>2</sub>	10 nm	2
F	15% $\mu$ SiO <sub>2</sub> +SiR	RTV-SiR	SiO <sub>2</sub>	3 $\mu$ m	15

where P, A, E, and L represent the applied load, cross-sectional area, strain at failure, and gauge length, respectively.

Shore A Duo (Durotech) equipment was used to measure hardness as per the ASTM D2240 standard [33]. All hardness tests were performed on square-shaped samples (50 × 50 × 3.5 mm) and the average of three blends of the same composition is reported.

### 2.3.2. Thermal characterization

Percentage weight loss and thermal stability of prepared blends were measured using a thermal analyzer (Shimadzu TGA-50H, Japan) at 20 °C/min heating rate in the temperature range of 0–850 °C. All tests were conducted on samples of 20 mg in air ambiance by fixing the sample between two temperature-controllable flat plates to provide uniform heat flow. The 10%, 50%, and final residual weight temperatures were measured under steady-state conditions for each sample.

### 2.3.3. Electrical characterization: IPT setup for tracking/erosion analysis

Various accelerated tests were employed to predict the performance and life of SiR-blends on HV transmission and distribution insulators. To evaluate the capacity of SiR composites to resist surface tracking and erosion, the ASTM D2303 IPT and erosion test was employed [34]. Figure 2 shows the setup of the IPTs with variable AC voltage source as per standard requirements. Each sample of size 65 × 25 × 3.5 mm was energized from a 220 V, 50 Hz AC voltage source with 70 kVA/10 kV variable transformer. In this test setup, the composite samples were mounted at an angle of 45° with respect to a horizontal line along with contamination (NH<sub>4</sub>CL with concentration of 1 g/dm<sup>3</sup> of distilled water) flow rate of 0.20 mL/min. The sample under test was observed after each passing hour; if the sample under test did not track, then the applied voltage was increased by 250 V. In subsequent stages, the same procedure was followed until continuous tracking of 25 mm deep on the insulator's surface or leakage current of more than 60 mA for 2 s was observed [35]. Furthermore, if the sample did not track in 6 h, the test was stopped as required by the ASTM D2303 standard. In addition, measurement of the surface temperature distribution was recorded by Fluke-Ti25 infrared (IR) camera at equal intervals of time, whereas leakage current (LC) was measured using a Fluke-digital multimeter between sample and ground terminal. As proposed by the standard, before and after testing, all the specimens were cleaned with distilled water and alcohol (isopropyl) and weighed. The percentage of eroded mass was calculated using the following equation [36]:

$$\% \text{ Eroded mass} = [( \text{final mass} - \text{initial mass} ) / \text{initial mass}] \times 100. \quad (3)$$

## 3. Results and discussion

### 3.1. Mechanical results

Mechanical properties like average TS, %EAB, and hardness of SiR-blends are compared in Figures 3, 4, and 5, respectively. It can be seen that blending of ATH and SiO<sub>2</sub> particles with SiR can result in enhanced mechanical features. The improved tensile strength of ATH/SiO<sub>2</sub> and ATH-SiO<sub>2</sub>-cofilled SiR-blends are presented in Figure 3. This improvement is 42.5% for blend-B, 470% for blend-C, 463% for blend-D, 256.25% for blend-E, and 125% for blend-F. Among all blends, only blend-C showed higher tensile strength of ~4.56 MPa, as depicted in Figure 3, which may be due to higher cross-linking (intense hydrogen bond between –OH groups of base rubber and filler surface groups) among the SiR matrix and ATH particles. Another reason may be the smaller free volume as well as particle uniform dispersion in the polymer matrix, which restricts chain mobility and consequently improves the tensile property.

Likewise, %EAB (which acts as an insulant degradation indicator) of all prepared blends was decreased with the addition of both ATH and silica particles in different wt.% as summarized and compared in Figure 4. This decrease in EAB is 55.60% for blend-B, 58.65% for blend-C, 23.68% for blend-D, 36.4% for blend-E, and 14.9% for blend-F. Maximum %EAB was exhibited by blend-C, as shown in Figure 4. This decreasing

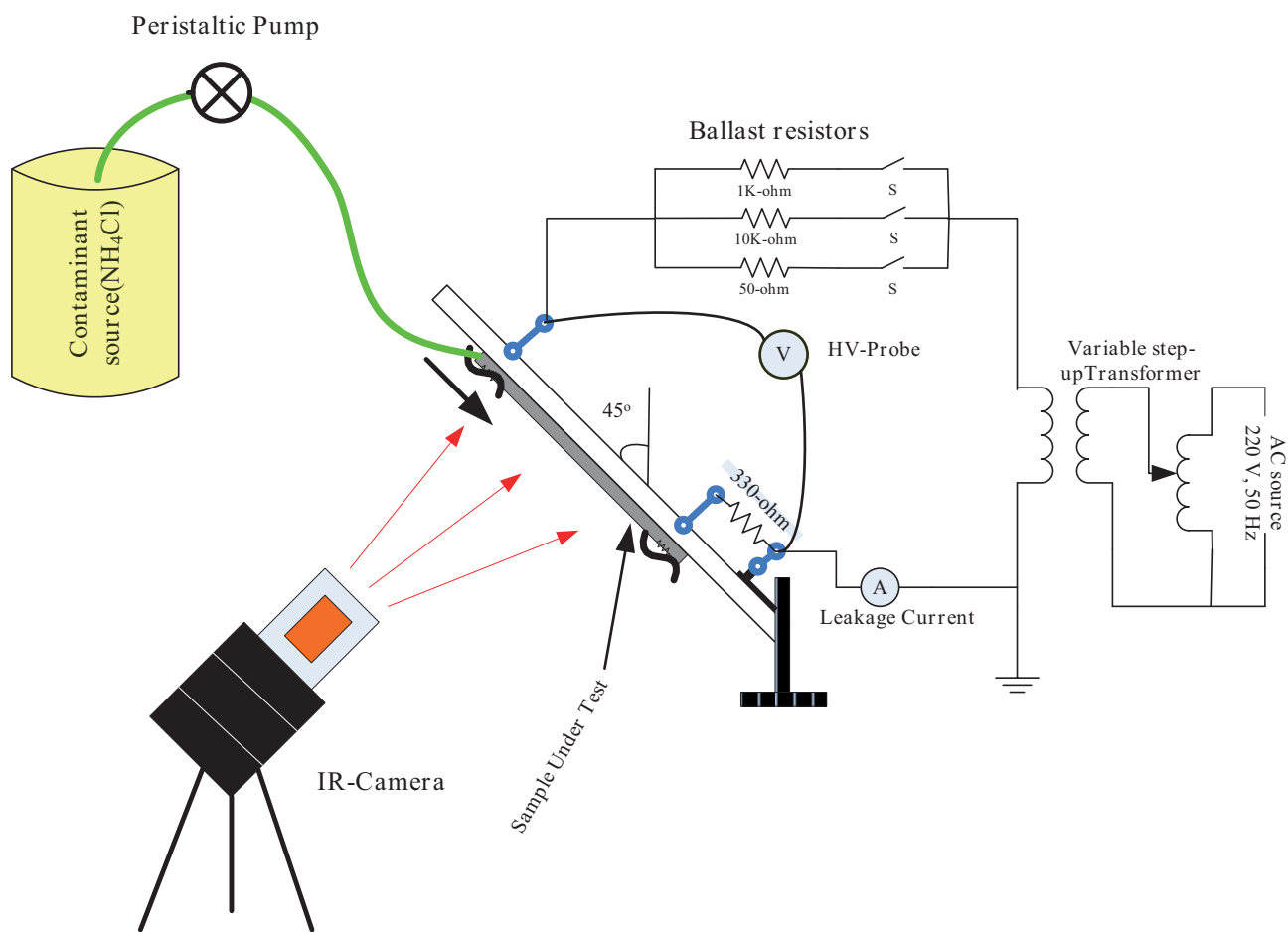


Figure 2. IPT setup.

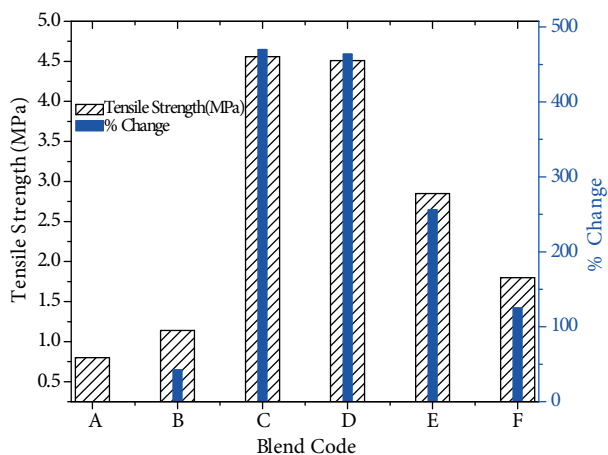
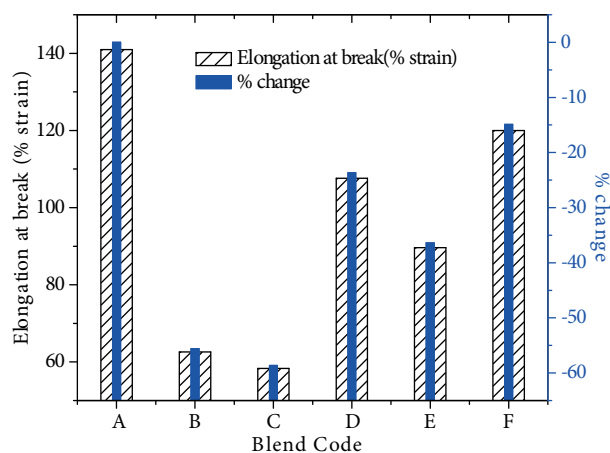
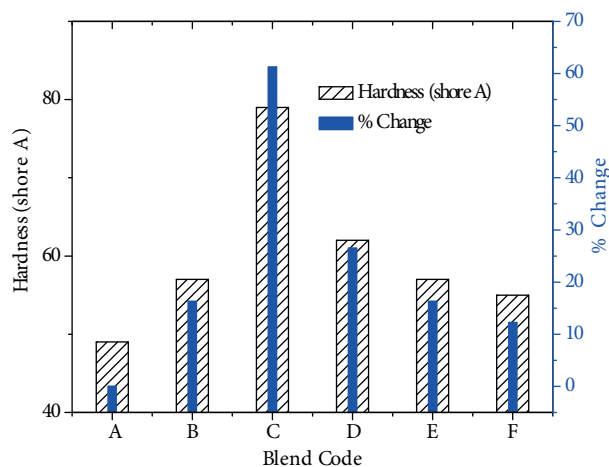


Figure 3. Tensile strength and % change of SiR-blends.

trend in %EAB of SiR-blends is attributed to smaller interparticle distances, strong bond energy, and enhanced cross-linking, which restrain chain scission and molecular instabilities.



**Figure 4.** Elongation at break and % change of SiR-blends.



**Figure 5.** Hardness and % change of SiR-blends.

Similarly all SiR-blends showed improvement in hardness with the addition of ATH/SiO<sub>2</sub> particles in different wt.%. This hardness improvement is 16.32% for blend-B, 61.22% for blend-C, 26.5% for blend-D, 16.32% for blend-E, and 12.24% for Blend-F as shown in Figure 5. From Figure 5, it is obvious that higher hardness was exhibited by blend-C (~79, shore A) compared to neat and all other SiR samples. This enhancement is attributed to particles' small size, uniform dispersion, higher molecular interactions, and improved cross-linking among particles and base matrix. Hence, generally all SiR-blends showed improved mechanical properties, but blend-C (20%  $\mu$ ATH) exhibited excellent mechanical properties.

### 3.2. TGA studies

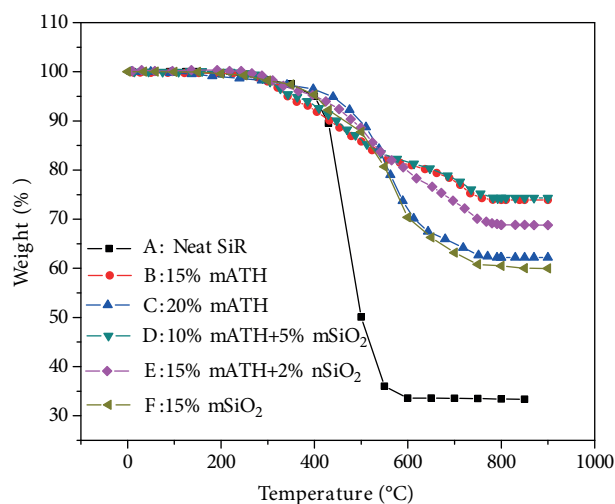
To understand the impact of ATH and SiO<sub>2</sub> particles on thermal performance of SiR-blends, TGA was conducted, as shown in Figure 6. From TGA curves (Figure 6), it is obvious that some samples exhibit superior performance and some have degraded behavior compared to neat SiR for the given temperature range (0–850 °C). Thermal stability of SiR is increased for blend-B and blend-D, whereas blends E, C, and F showed degraded performance compared to neat SiR. For instance, at 850 °C, the final residual wt.% left for blends A, B, C, D, E, and F are 69.24%, 73.92%, 62.19%, 74.31%, 68.81%, and 59.98%, respectively (Figure 6). Among all composites, blend-D exhibited the highest residuary mass (74.31%), whereas lowest mass was found for blend-F (59.98%). This variation in mass loss and final residuary is due to the material decomposition, chain scission, evaporation of volatile species, moisture, and gas particles. Blends' thermal degradation may be due to CH<sub>3</sub>-group oxidation, depolymerization, increased molecular interactions between the SiR matrix and ATH/SiO<sub>2</sub> particles at elevated temperature, and covalent bond amalgamation (H-bond). Consequently, reduction in cross-linking as well as van der Waals forces can be exhibited by SiR-blends at higher temperatures. Hence, from TGA analysis, we infer that hybrid particles (ATH+SiO<sub>2</sub>) in certain proportions have significant impact on SiR thermal characteristics as validated by the blend-D composition.

### 3.3. Electrical properties

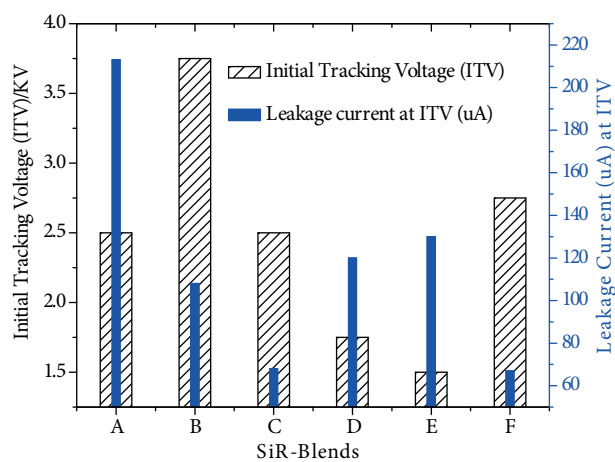
#### 3.3.1. Tracking/erosion analysis results

The initial tracking voltage (ITV) and corresponding leakage current (LC) obtained for polymer samples are figured as a function of SiR-blends as shown in Figure 7. It can be noted that ITV is independent of particle

concentration (wt.%) and depends on energy dissipation in SiR-blends [37]. From Figure 7, it can be seen that ITV and LC vary in discrete proportion to ATH/SiO<sub>2</sub>-filled SiR-blends. Measured values are 2.5 kV, 3.75 kV, 2.56 kV, 1.75 kV, 1.5 kV, and 2.75 kV for blends A, B, C, D, E, and F, respectively. Among all the investigated samples, the maximum ITV is exhibited by blend-B compared to other SiR-blends. During tests, execution chalking and hydrophobicity variation were also noticed in direct proportion to the applied voltage and test execution time on the top surface of SiR-blends. In addition, the ammonium-chloride (NH<sub>4</sub>CL) contaminant during IPTs bridges the top and bottom electrodes, which causes surface conductivity and joule-heating effect. As a consequence, the dry band arcing is formed as soon as the input voltage exceeds the sample breakdown voltage, as validated by the blends' thermographs (Figure 8). During the arcing period the generated heat is conducted from arc to specimen surface, which yields caloric/thermal deterioration and transforms samples from hydrophobic to hydrophilic, as demonstrated in Figure 8. These thermographs of SiR-blends were recorded during IPTs to investigate surface tracking, thermal profile, and hydrophobicity variation with time. From IR images, it is obvious that dry band arcing varies along the sample surface with time, which eventually increases surface as well as surrounding temperatures through diffusion of heat. Among all IR images of fabricated blends, it is inferred that upon gradual increase in voltage with time, minimum time-to-track was exhibited by blend-E (60 min), whereas maximum time-to-track was noticed for blend-B (300 min). In IR images, the red and bright spots denote higher temperature whereas blueish spots indicate lower temperature.



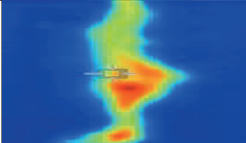
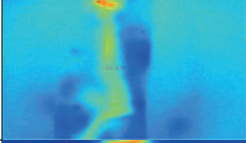
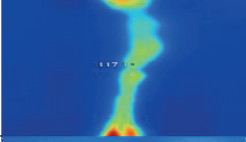
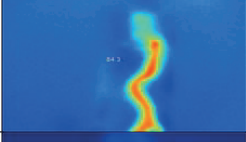
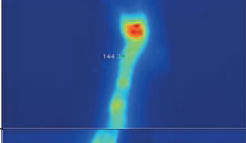
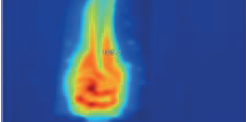
**Figure 6.** TGA curves of SiR-blends.



**Figure 7.** Initial tracking voltage and leakage current of SiR-blends.

Moreover, in consequence of continuous arcing, enough energy can be transferred to the sample surface, which accelerates material decomposition as well as erosion as depicted in Figure 9. Herein, it can be seen that SiR-blends' mass loss varies with filler type and concentration, which is 2.5% for blend-A, 1.43% for blend-B, 3.81% for blend-C, 7.1% for blend-D, 27.4% for blend-E, and 0.5% for blend-F. Among all investigated samples, maximum erosion takes place in blend-E (~1500 mg), whereas minimum mass loss was found in blend-F (~31 mg), as shown in Figure 9. The SiR-blends with ATH (B, C, D, E) showed higher mass loss compared to SiR-SiO<sub>2</sub> blends. This is attributed to variation in bond energies among ATH/SiO<sub>2</sub> and the SiR matrix. In addition, the heat generated during arcing and its conduction from the tracked region to the surrounding environment also influences the erosion of the polymeric blends, which varies for silica as well as



Blend type	IR -image	Tracking Time (min)	Tracking Temperature
A		180	56 °C
B		300	39 °C
C		240	43 °C
D		120	72 °C
E		60	78 °C
F		240	49 °C

**Figure 8.** IR images, tracking time, and maximum temperature of SiR-blends.

ATH samples as validated by IR thermographs. Furthermore, while performing erosion/tracking tests, gradual decrease in sample hydrophobicity with time was noticed for all blends, but rapid hydrophobicity loss was found for blend-E as indicated by IR images. This hydrophobicity loss may be due to evaporation and diffusion of low-molecular-weight particles from the bulk of material to the outer surface.

### 3.3.2. Correlation between electrical and mechanical properties

Hydrophobicity, hardness, tensile strength, dielectric strength, erosion, and tracking resistance are material physical properties. These properties vary even among identical polymer samples due to internal defects, filler type/concentrations, and molecular conformations [28]. In the literature there is no direct mathematical relationship between mechanical and electrical properties. However, on the basis of the literature it can be correlated as follows.

The dielectric breakdown property (i.e. the maximum voltage that an insulation material can sustain) of any insulating material depends on the intensity of applied electric field (voltage), which can be calculated using the following formula [29,30]:

$$\text{Dielectric strength (kV/mm)} = \text{Breakdown voltage (kV)/sample thickness (mm)} \quad (4)$$

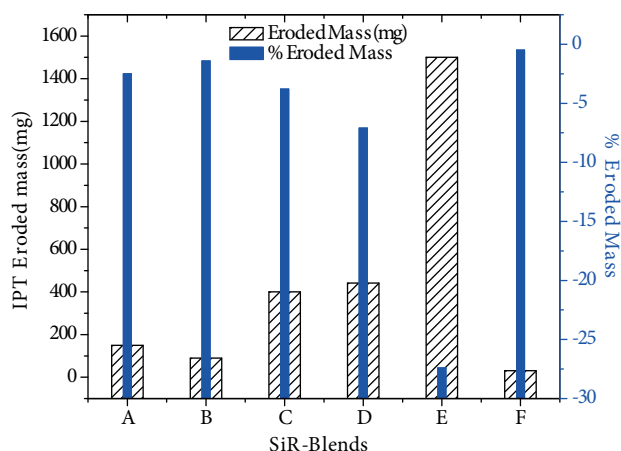


**Figure 9.** IPT eroded mass and % eroded mass of SiR-blends.

Likewise, Swanson et al. [31] correlated the dielectric strength with volume/surface resistivity, relative permittivity, and loss tangent according to the following formulas:

$$\text{Dielectric strength (kV/mm)} = A + [B \times \log(\rho v / (\zeta r \times \tan \varphi))], \quad (5)$$

where  $\rho v$  is the volume resistivity,  $\zeta r$  is the relative permittivity, and  $\tan \varphi$  is the loss tangent, and

$$\text{Volume resistivity } (\rho v) = [1 / (n \times \mu \times e)], \quad (6)$$

where  $n$  is the number of charge carriers,  $\mu$  is the charge mobility, and  $e$  is the particle charge.

It can be seen from Eq. (6) that there is an inverse relationship between volume resistivity and charge mobility. Now, as soon as the applied electric field (applied voltage) across the polymer samples increases, the corona discharge generates ionic particles and energetic electrons, ultraviolet, ozone, etc. Consequently these particles will cause the degradation of macromolecular chains into low-weight molecules due to chemical bonds breaking [32,33]. Hence, with the increase in surface discharges due to applied voltage, the increased crosslinking process prevents the low-weight molecules from transferring from the bulk of the material to the surface, which leads to a reduction in hydrophobicity and mechanical stability [34]. This reduction in surface hydrophobicity due to electrical and nonelectrical stresses could speed up the surface deterioration and physical defects (pores and flaws), thereby reducing surface/volume resistivities. As a consequence, it induces LC and dry band arc discharges on SiR specimens [35]. This LC gives us good indications about mechanical and surface degradation processes, because there is a direct relationship between LC and surface hydrophobicity (resistivity), as was observed during tracking/erosion investigations (Section 3.3.1) of SiR-blends.

In addition, electrical (i.e. arcing, corona discharge, leakage current) and environmental (i.e. heat, UV-radiation, wind, biological degradation, snow, acid rain) stresses have significant effects on insulation mechanical, thermal, and electrical properties [36,37]. As electrical stress occurs on insulator surface, it leads to the degradation of electrical characteristics, which is due to the loss of low-molecular-weight components and volatile particles. Likewise, environmental stresses such as UV, heat, snow, acid rain, and biological factors depolymerize polymer insulants and scission of Si-O-Si chains. Consequently, loss of elasticity, erosion, and surface roughness take place, which leads to reduction in mechanical stability. Hence, it can be inferred that due to electrical and environmental stresses there is a direct relationship between electrical and mechanical

properties as validated by IPTs and IR images. During IPT operations, a gradual decrease in hydrophobicity (resistance to water absorption and flow) followed by increase in LC was observed. As soon as samples lost their surface resistivity, tracking occurred, followed by erosion and weak mechanical performance.

#### 4. Conclusions

In summary, RTV-SiR composites filled with micro-ATH and micro- and nanosized silica particles were prepared and investigated for mechanical, thermal, tracking, and erosion properties. The amalgamation of micro/nanoparticles into the SiR base matrix imparted enhanced mechanical, thermal, and electrical properties. The major conclusions are summarized as follows.

Mechanically, compared to all other SiR composites, blend-C showed higher tensile strength ( $\sim 4.56$  MPa), reduced elongation at break ( $\sim 58.3\%$  strain), and improved hardness ( $\sim 79$ ).

Thermally, the hybrid blend-D exhibited excellent thermal stability by leaving higher residual mass (74.3%) at  $850^\circ\text{C}$  than that of other SiR-blends. In addition, at  $850^\circ\text{C}$  the neat SiR sample showed inferior thermal stability, leaving lower residual mass (33%).

Electrically, enhancement in tracking and erosion resistance was found both for ATH and silica-filled blends. However, in comparison to the ATH/SiO<sub>2</sub>-filled SiR composites, the maximum tracking resistance was demonstrated by blend-B at  $\sim 3.75$  kV. Likewise, the maximum erosion resistance (lower eroded mass) was computed for blend-F (31 mg), which is much lower than in all SiR specimens.

Hence, from silicone rubber novel blends, it is inferred that micro-ATH blends showed enhanced mechanical and tracking performance, while the hybrid blend (D) and SiO<sub>2</sub>-filled blend (F) exhibited higher thermal stability and erosion resistance, respectively. These characterization results will satisfy the applications of SiR insulants in the field of electronic and electrical engineering.

#### Acknowledgments

The authors would like to express their gratitude to the management of Marine Systems Limited (MSL), Pakistan, for providing the testing facilities. The authors would also like to acknowledge the valuable suggestions of Professor Raji Sundararajan of Purdue University, USA.

#### References

- [1] Ramirez I, Cherney EA, Jarayam S. Comparison of the erosion resistance of silicone rubber and EPDM composites filled with micro silica and ATH. *IEEE T Dielect El In* 2012; 19: 218-224.
- [2] Song W, Shen WW, Zhang GJ, Song BP, Lang Y, Su GQ. Aging characterization of high temperature vulcanized silicone rubber housing material used for outdoor insulation. *IEEE T Dielect El In* 2015; 22: 961-969.
- [3] Moghadam MK, Morshedian J, Ehsani M, Laine RM, Kuang LY, Umehara N. Effects of Ph<sub>12</sub>SQ on the thermal stability and mechanical properties of high temperature vulcanized (HTV) silicone rubber. *IEEE T Dielect El In* 2014; 21: 244-252.
- [4] Jun-Wei Z, Zhi-Min D, Wei-Kang L, Yan-Hui Z, Chen G. Effect of micro-Si<sub>3</sub>N<sub>4</sub>-nano-Al<sub>2</sub>O<sub>3</sub> co-filled particles on thermal conductivity, dielectric and mechanical properties of silicone rubber composites. *IEEE T Dielect El In* 2014; 21: 1989-1996.
- [5] Yanfeng G, Jiafu W, Xidong L, Zhipeng Y, Yingyan L, Yuanji C. Investigation on permeation properties of liquids into HTV silicone rubber materials. *IEEE T Dielect El In* 2014; 21: 2428-2437.

- [6] Gorur R, Cherney EA, Hackam R. Performance of polymeric insulating materials in salt-fog. *IEEE T Power Deliver* 1987; 2: 486-492.
- [7] Venkatesulu B, Thomas MJ. Erosion resistance of alumina-filled silicone rubber nanocomposites. *IEEE T Dielect El In* 2010; 17: 615-624.
- [8] Burditt N. Mineral fillers in polymers: a special review. In: Griffiths J, editor. 10th Industrial Minerals International Congress; 1991. p. 8.
- [9] Zhao T, Bernstorff RA. Ageing tests of polymeric housing materials for non-ceramic insulators. *IEEE Electr Insul M* 1998; 2: 26-33.
- [10] Ansorge S, Schmuck F, Aitken S, Papailiou K. Improved performance of silicone rubbers for the use in composite insulators. In: 2010 CIGRE; 2010; Paris, France.
- [11] Ramirez I, Cherney EA, Jarayam S. Comparison of the erosion resistance of silicone rubber and EPDM composites filled with micro silica and ATH. *IEEE T Dielect El In* 2012; 19: 218-224.
- [12] Vas JV, Venkatesulu B, Thomas MJ. Tracking and erosion of silicone rubber nanocomposites under DC voltages of both polarities. *IEEE T Dielect El In* 2012; 19: 91-98.
- [13] Dickstein W, Siemens R, Hadziioannou E. Dynamic mechanical and thermogravimetric analyses of the effect of ferric oxide on the thermaloxidative degradation of silicone rubber. *Thermochim Acta* 1990; 166: 137-145.
- [14] Meyer LH, Cherney EA, Jayaram SH. The role of inorganic fillers in silicone rubber for outdoor insulation alumina tri-hydrate or silica. *IEEE Electr Insul M* 2004; 20: 13-21.
- [15] Wang X, Nelson JK, Schadler LS, Hillborg H. Mechanisms leading to nonlinear electrical response of a nano p-SiC/silicone rubber composite. *IEEE T Dielect El In* 2010; 17: 1687-1696.
- [16] Zha LW, Zhu YH, Li WK, Bai J, Dang ZM. Low dielectric permittivity and high thermal conductivity silicone rubber composites with micro-nano-sized particles. *Appl Phys Lett* 2012; 101: 062905.
- [17] Zha JW, Dang ZM, Li WK, Zhu YH, Chen G. Effect of micro-Si<sub>3</sub>N<sub>4</sub>-nano-Al<sub>2</sub>O<sub>3</sub> co-filled particles on thermal conductivity, dielectric and mechanical properties of silicone rubber composites. *IEEE T Dielect El In* 2014; 21: 1989-1996.
- [18] Prabu RR, Usa S, Udayakumar K, Abdullah M, Majeed SSM. Electrical Insulation characteristics of silicone and EPDM polymeric blends. I. *IEEE T Dielect El In* 2007; 14: 1207-1214.
- [19] Iida K, Hackam R. Effect of low molecular weight fluid on the surface free energy of an alloy of EPDM/SIR. In: *IEEE 2005 International Symposium on Electrical Insulating Materials*; 5-9 June 2005. pp. 352-355.
- [20] Cherney EA. Nanodielectrics applications-today and tomorrow. *IEEE Electr Insul M* 2013; 29: 59-65.
- [21] Du BX, Xu H. Effects of thermal conductivity on dc resistance to erosion of silicone rubber/BN nanocomposites. *IEEE T Dielect El In* 2014; 21: 511-518.
- [22] Ansorge S, Schmuck F, Papailiou KO. Impact of different fillers and filler treatments on the erosion suppression mechanism of silicone rubber for use as outdoor insulation material. *IEEE T Dielect El In* 2015; 22: 979-988.
- [23] Meyer LH, Jayaram SH, Cherney EA. A novel technique to evaluate the erosion resistance of silicone rubber composites for high voltage outdoor insulation using infrared laser erosion. *IEEE T Dielect El In*; 12: 1201-1208.
- [24] Schmidt LE, Kornmann X, Krivda A, Hillborg H. Tracking and erosion resistance of high temperature vulcanizing ATH-free silicone rubber. *IEEE T Dielect El In* 2010; 17: 533-540.
- [25] Du B, Xu H. Effects of thermal conductivity on dc resistance to erosion of silicone rubber/BN nanocomposites. *IEEE T Dielect El In* 2014; 21: 511-518.
- [26] Kumar R, Gupta N. Tracking and surface degradation of barium titanate filled silicone rubber nanocomposites. In: *IEEE 2015 Conference on Electrical Insulation and Dielectric Phenomena*; 2015. pp. 495-498.
- [27] Ghunem RA, Jayaram SH, Cherney EA. Suppression of silicone rubber erosion by alumina trihydrate and silica fillers from dry-band arcing under DC. *IEEE T Dielect El In* 2015; 22:14-20.

- [28] Zhou W, Wang C, Ai T, Wu K, Zhao F, Gu H. A novel fiber-reinforced polyethylene composite with added silicon nitride particles for enhanced thermal conductivity. *Compos Part A-Appl S* 2009; 40: 830-836.
- [29] Khan H, Amin M, Ali M, Iqbal M, Yasin M. Effect of micro/nano-SiO<sub>2</sub> on Mechanical, thermal and electrical properties of silicone rubber, epoxy and EPDM composites for outdoor electrical insulations. *Turk J Electr Eng Co* 2017; 25: 1426-1435.
- [30] ASTM International. ASTM D1418-10a. Standard Practice for Rubber and Rubber Lattices Nomenclature. West Conshohocken, PA, USA: ASTM International, 2010.
- [31] ASTM International. ASTM D412-15a. Standard Test Methods for Vulcanized Rubber and Thermoplastic Elastomers—Tension. West Conshohocken, PA, USA: ASTM International, 2015.
- [32] Khalil A, Zahid Raza N, Shirin K. Cure characteristics, mechanical and swelling properties of marble sludge filled EPDM modified chloroprene rubber blends. *Advances in Material Physics and Chemistry* 2012; 2: 90-97.
- [33] ASTM International. ASTM D2240-10. Standard Test Method for Rubber Property-Durometer Hardness. West Conshohocken, PA, USA: ASTM International, 2010.
- [34] ASTM International. ASTM D2303. Standard Test Method for Liquid Contaminant, Inclined Plane Tracking and Erosion of Insulating Materials. West Conshohocken, PA, USA: ASTM International, 2004.
- [35] Kumagai S, Yoshimura N. Influence of single and multiple environmental stresses on tracking and erosion of RTV silicone rubber. *IEEE T Dielect El In* 1999; 6: 211-225.
- [36] Ghunem RA, Jayaram SH, Cherney EA. Investigation into the eroding dry-band arcing of filled silicone rubber under DC using wavelet-based multiresolution analysis. *IEEE T Dielect El In* 2014; 21: 713-720.
- [37] Ghunem RA, Jayaram SH, Cherney EA. Erosion of silicone rubber composites in the AC and DC inclined plane tests. *IEEE T Dielect El In* 2013; 20: 229-236.